

to drive the oxidation reaction at room temperature. For photocatalytic aerobic oxidation of benzylic carbon centres, homogeneous catalysts (e.g. Mn^{III} corrolazine complex,¹⁹ 2,3-dichloro-5,6-dicyano-1,4-benzoquinone³²) with co-catalysts and heterogeneous catalysts (e.g. $g\text{-C}_3\text{N}_4$, CdS^{20}) have been tested. In this work, we report such a process using 1 bar O_2 and CNNS/MFM-300(Fe) for the photocatalytic oxidation of xanthene using visible light at room temperature (Fig. 2a). Toluene is the most suitable solvent compared with MeCN and trifluorotoluene for this atom efficient process for a range of substrates (Table 1). A CNNS/MFM-300(Fe) composite with a $g\text{-C}_3\text{N}_4$ content of 70 wt% shows the best catalytic activity (Fig. S8 and S9, ESI[†]). The conversion of xanthene reaches >99% within 5 h with a xanthone selectivity of >99% (Fig. 2a). The turnover frequency (TOF)³³ ($3.28 \text{ mol kg}^{-1} \text{ h}^{-1}$; mol of product, per kg of catalyst, per hour) for this reaction over 5 h is significantly higher than those of previously reported reactions conducted with the strong oxidant *tert*-butyl hydroperoxide (tBuOOH) and MOF catalysts at 343 K: $[\text{Fe}(\text{BTC})_3]$ (TOF = $0.15 \text{ mol kg}^{-1} \text{ h}^{-1}$), $[\text{Cu}_3(\text{BTC})_2]$ (TOF = $0.12 \text{ mol kg}^{-1} \text{ h}^{-1}$), $[\text{Al}_2(\text{BDC})_3]$ (TOF = $0.06 \text{ mol kg}^{-1} \text{ h}^{-1}$) (BTC³⁻ = benzene-1,3,5-tricarboxylate; BDC²⁻ = 1,4-benzendicarboxylate), iron citrate (TOF = $0.60 \text{ mol kg}^{-1} \text{ h}^{-1}$), and Fe-exchanged Y zeolite (TOF = $0.006 \text{ mol kg}^{-1} \text{ h}^{-1}$).³³ The high stability of CNNS/MFM-300(Fe) was confirmed by cycling experiments, with only a very small reduction in yield of xanthone observed over five cycles of photocatalysis (Fig. 2b). The PXRD pattern of CNNS/MFM-300(Fe) after five cycles of photoreaction confirms the retention of crystallinity and structure of MFM-300(Fe) (Fig. S10, ESI[†]). A leaching test was performed by removing the

catalyst from the reaction mixture after 0.5 h. On removal of catalyst a significant drop in reaction rate was observed, thus confirming the key role of CNNS/MFM-300(Fe) and the absence of significant leaching of active sites into solution (Fig. S11, ESI[†]). The CNNS/MFM-300(Fe) composite also shows high activity and selectivity for the oxidation of indane, thioxanthene and fluorene at room temperature under visible light, demonstrating its general applicability (Table 1). The present system unfortunately shows poor activity toward the oxidation of acyclic benzylic derivatives such as ethylbenzene. Under the same conditions, bulk $g\text{-C}_3\text{N}_4$ and MFM-300(Fe) can individually catalyse the conversion of xanthene (Fig. 2a), but both show poorer catalytic activity compared with the composite, with values for TOF of 1.34 and $0.49 \text{ mol kg}^{-1} \text{ h}^{-1}$ over 5 h, respectively. Poor dispersion of MOF in $g\text{-C}_3\text{N}_4$ was observed when the synthesis of the composite was attempted in the absence of CO_2 or CTAB (Fig. S12 and S13, ESI[†]), and the catalytic activity of the resultant $g\text{-C}_3\text{N}_4\text{-MFM-300(Fe)}$ mixture is much lower than that of the composite prepared in the optimal way (Table 1 and Fig. 2a). This suggests that the high activity of the CNNS/MFM-300(Fe) composite originates from the interface between the two components at and within the heterojunction. When reactions were conducted in dark, negligible catalysis was observed, indicating that the reaction follows a photocatalytic mechanism.

Photocatalysis mechanism study

To rationalise the high catalytic performance of CNNS/MFM-300(Fe), the energy of the optical band gap for MFM-300(Fe), bulk $g\text{-C}_3\text{N}_4$, CNNS and the CNNS/MFM-300(Fe) composite were

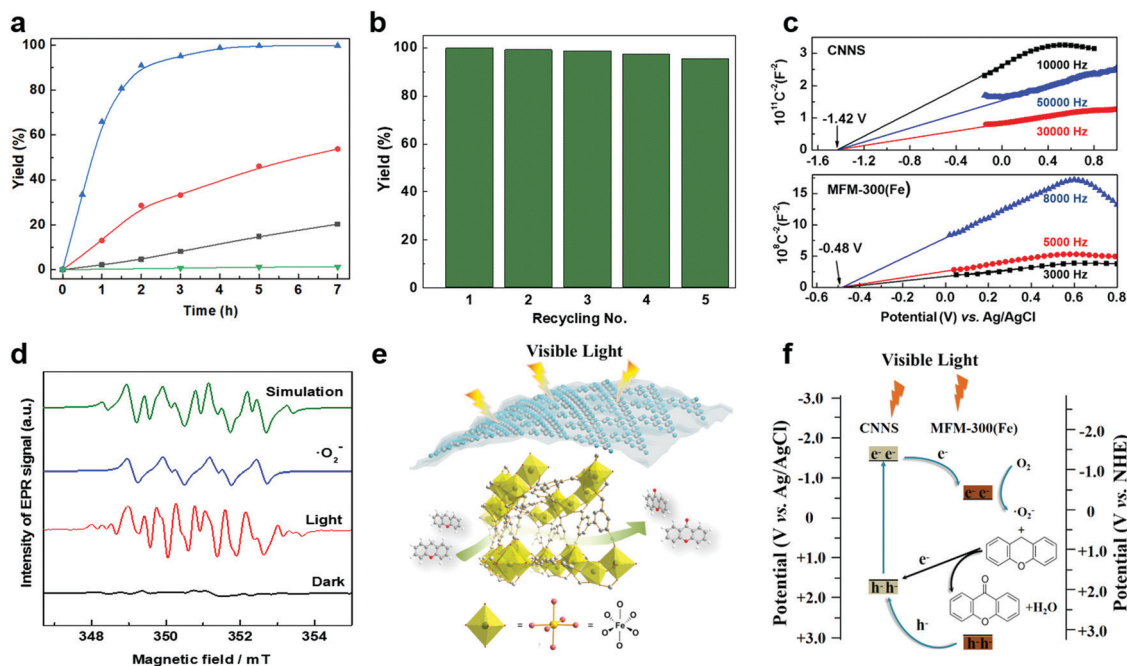
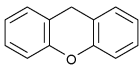
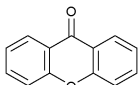
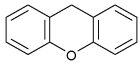
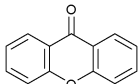
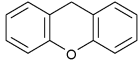
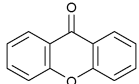
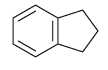
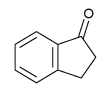
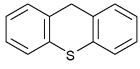
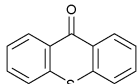
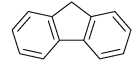
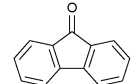
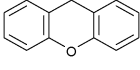
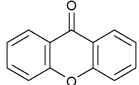
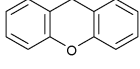
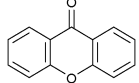
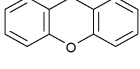
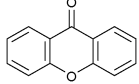
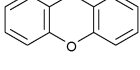
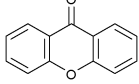
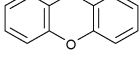
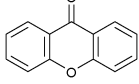


Fig. 2 (a) Formation of xanthone catalysed by MFM-300(Fe) (black), $g\text{-C}_3\text{N}_4$ (red), CNNS/MFM-300(Fe) composites (blue) and thermal catalysis with CNNS/MFM-300(Fe) composites at 343 K in the dark (green). (b) Catalytic performance over five continuous cycles of oxidation of xanthene. (c) Mott–Schottky plots for CNNS (top) and MFM-300(Fe) (bottom) at different frequencies. (d) EPR spectra spin-trapping with DMPO of CNNS/MFM-300(Fe) under dark conditions (black) and after 10 min of visible light irradiation (red). Signals for $\cdot\text{O}_2^-$ (blue) and simulated (green) of the spectrum after irradiation. (e) Schematic diagram for the photocatalytic process. (f) Schematic illustration of charge separation of CNNS and MFM-300(Fe) and charge-transfer between the bands of CNNS/MFM-300(Fe) heterojunctions. The CNNS/MFM-300(Fe) composites shown here contain $g\text{-C}_3\text{N}_4$:MOF in a wt:wt ratio of 7:3.



Table 1 Photocatalytic conversion of aromatic substrates using CNNS/MFM-300(Fe) composites in the presence of O₂ at 298 K

Entry	Substrate	Product	Time (h)	Conversion (%)	Selectivity (%)	TOF (mol h ⁻¹ kg ⁻¹)
1 ^a			5	>99.0	>99	3.28
2 ^b			5	47.9	>99	1.59
3 ^c			5	59.3	>99	1.95
4			24	91.0	85	0.37
5			13	96.2	>99	1.12
6			24	87.3	95	0.46
7 ^d			5	52.3	88	1.52
8 ^e			5	14.9	>99	0.49
9 ^f			5	41.5	91	1.25
10 ^g			5	2.2	>99	0.07
11 ^h			5	0.3	>99	0.01

^a Reaction conditions: xanthene (30 mg), CNNS/MFM-300(Fe) (10 mg) (g-C₃N₄:MOF in a wt:wt ratio of 7:3), toluene (4 mL), O₂ (1 bar), λ > 400 nm, 298 K. ^b Xanthene (30 mg), CNNS/MFM-300(Fe) (10 mg) (g-C₃N₄:MOF in a wt:wt ratio of 7:3), MeCN (4 mL), O₂ (1 bar), λ > 400 nm, 298 K. ^c Xanthene (30 mg), CNNS/MFM-300(Fe) (10 mg) (g-C₃N₄:MOF in a wt:wt ratio of 7:3), trifluorotoluene (4 mL), O₂ (1 bar), λ > 400 nm, 298 K. ^d With bulk g-C₃N₄ as the photocatalyst (10 mg), xanthene (30 mg), toluene (4 mL), O₂ (1 bar), λ > 400 nm, 298 K. ^e With MFM-300(Fe) as the photocatalyst (10 mg), xanthene (30 mg), toluene (4 mL), O₂ (1 bar), λ > 400 nm, 298 K. ^f g-C₃N₄/MFM-300(Fe) composite synthesised without CO₂ or CTAB as the photocatalyst (10 mg), xanthene (30 mg), toluene (4 mL), O₂ (1 bar), λ > 400 nm, 298 K. ^g Without a catalyst, xanthene (30 mg), toluene (4 mL), O₂ (1 bar), λ > 400 nm, 298 K. ^h Without light, CNNS/MFM-300(Fe) (10 mg) (g-C₃N₄:MOF in a wt:wt ratio of 7:3), xanthene (30 mg), toluene (4 mL), O₂ (1 bar), λ > 400 nm, 298 K. Other reaction conditions without notes are the same as that used for (a).

determined by electronic spectroscopy to be 3.25, 2.90, 2.99 and 2.97 eV, respectively, using the Tauc-plot method (Fig. S14, ESI[†]). The flat-band potentials derived from Mott-Schottky plots in the dark are -0.48(3) V and -1.42(4) V vs. Ag/AgCl for MFM-300(Fe) and CNNS (Fig. 2c), respectively, suggesting a strong driving force for the photo-excited electrons from CNNS to transfer to MFM-300(Fe). The appropriate band alignment between CNNS and MFM-300(Fe) thus appears to satisfy the thermodynamic requirements for the separation of charge at the interface.

In thermal-catalysed oxidation of hydrocarbons with O₂, lattice oxygen in the metal oxide catalysts first transfers from the catalyst to the hydrocarbon and the reduced catalyst is

subsequently oxidised by O₂.³⁴ We rationalised that the formation of reactive radicals would account for the observed photocatalytic oxidation of benzylic carbons, and we therefore sought to probe the formation of such radicals by EPR spectroscopy *via* spin-trapping experiments. The catalyst CNNS/MFM-300(Fe) suspended in anhydrous toluene gave only very weak EPR spectra in the presence of the spin trap DMPO and molecular O₂ (1 bar) under dark conditions (Fig. 2d and Fig. S16 and S17, ESI[†]). On irradiation with visible light, strong EPR spectra were obtained confirming the generation of radical species. The spectra are dominated by the characteristic spectrum of the superoxide adduct DMPO•O₂⁻ (Fig. 2d and



- 24 H. X. Zhao, H. T. Yu, X. Quan, S. Chen, H. M. Zhao and H. Wang, *RSC Adv.*, 2014, **4**, 624.
- 25 X. Zhang, I. da Silva, H. G. W. Godfrey, S. K. Callear, S. A. Sapchenko, Y. Cheng, I. Vitorica-Yrezabal, M. D. Frogley, G. Cinque, C. C. Tang, C. Giacobbe, C. Dejoie, S. Rudic, A. J. Ramirez-Cuesta, M. A. Denecke, S. Yang and M. Schröder, *J. Am. Chem. Soc.*, 2017, **139**, 16289.
- 26 S. Yang, J. L. Sun, A. J. Ramirez-Cuesta, S. K. Callear, W. I. F. David, D. P. Anderson, R. Newby, A. J. Blake, J. E. Parker, C. C. Tang and M. Schröder, *Nat. Chem.*, 2012, **4**, 887.
- 27 J. S. Zhang, M. W. Zhang, R. Q. Sun and X. C. Wang, *Angew. Chem., Int. Ed.*, 2012, **51**, 10145.
- 28 G. W. Zhang, S. Y. Huang, A. Chaves, C. Y. Song, V. O. Ozcelik, T. Low and H. G. Yan, *Nat. Commun.*, 2017, **8**, 14071.
- 29 K. G. M. Laurier, F. Vermoortele, R. Ameloot, D. E. De Vos, J. Hofkens and M. B. J. Roeffaers, *J. Am. Chem. Soc.*, 2013, **135**, 14488.
- 30 D. R. Sun, L. Ye and Z. H. Li, *Appl. Catal., B*, 2015, **164**, 428.
- 31 X. C. Kang, X. F. Sun, Q. G. Zhu, X. X. Ma, H. Z. Liu and B. X. Han, *Chem. Commun.*, 2016, **52**, 4687.
- 32 F. Rusch, J. C. Schober and M. Brasholz, *ChemCatChem*, 2016, **8**, 2881.
- 33 A. Dhakshinamoorthy, M. Alvaro and H. Garcia, *J. Catal.*, 2009, **267**, 1.
- 34 A. M. Khenkin, L. Weiner, Y. Wang and R. Neumann, *J. Am. Chem. Soc.*, 2001, **123**, 8531.
- 35 F. Z. Su, S. C. Mathew, L. Mohlmann, M. Antonietti, X. C. Wang and S. Blechert, *Angew. Chem., Int. Ed.*, 2011, **50**, 657.
- 36 R. Marschall, *Adv. Funct. Mater.*, 2014, **24**, 2421.

